Maximal wall shear stress in arterial stenoses: application to the internal carotid arteries

Sylvie Lorthois, Pierre-Yves Lagrée, Jean-Pierre Marc-Vergnes, Francis Cassot

Sylvie Lorthois
Institut de Mécanique des Fluides de Toulouse,
UMR CNRS 5502,
31400 Toulouse Cedex, France

Pierre-Yves Lagrée
Chargé de Recherche,
Laboratoire de Modélisation en Mécanique,
UMR CNRS 7607,
75252 Paris Cedex 5, France

Jean-Pierre Marc-Vergnes
Directeur de Recherche.

Francis Cassot
Chargé de Recherche.

I.N.S.E.R.M. U 455,
C.H.U. Purpan,
31059 Toulouse Cedex, France

Maximal Wall Shear Stress in Arterial Stenoses: Application to the Internal Carotid Arteries

Maximal wall shear stress (MWSS) in the convergent part of a stenosis is calculated by the interactive boundary-layer theory. A dimensional analysis of the problem shows that MWSS depends only on a few measurable parameters. A simple relationship between MWSS and these parameters is obtained, validated, and used to calculate the magnitude of MWSS in a carotid stenosis, as a function of the patency of the circle of Willis and the stenotic pattern. This demonstrates the huge effect of collateral pathways. Elevated MWSS are observed even in moderate stenoses, provided they are associated with a contralateral occlusion, a large anterior, and narrow posterior communicating arteries, suggesting a potential risk of embolus release in this configuration.

Keywords: Wall Shear Stress, Stenosis, Carotid Disease, Cerebral Circulation, Boundary-Layer

Introduction

Stenoses and occlusions of internal carotid arteries are involved in 34 [1] to 44 percent [2] of strokes. Large multicenter trials [3,4] have shown that the risk of stroke increases significantly with the degree of stenosis. Carotid lesions induce strokes by either a hemodynamic or an embolic mechanism. In the first case, obstructive lesions induce a loss of perfusion pressure that causes ischemic lesions in the downstream cerebral territories. Poor collateral arterial circulation through the circle of Willis (the main anastomotic network situated at the base of skull) has been shown to be frequently associated with this clinical condition [5,6]. In the case of embolic strokes, materials detached from ulcerated plaque or mural thrombus migrate from the stenosis and occlude the distal smaller vessels [7]. The embolization is probably related to complex biochemical phenomena in plaque and/or thrombus components, which determine their mechanical properties, but also to shear stress due to blood flow [8]. In a simulation study, Cassot et al. [9] showed that differences in collateral pathways of the circle of Willis and in degree of contralateral stenosis induce great interindividual variability of measurable parameters (flow rate, velocity) in a stenosis of a given radius reduction. They suggested that this variability could lead to large changes in maximal wall shear stress (MWSS) that could play a role in the embolic mechanism. However, the magnitude of these shear stress variations has still to be quantified.

In spite of abundant literature about magnitude and effects of wall shear stresses at early stages of development of atherosclerosis and mural thrombosis [10–12], there is no report about the evaluation of high shear stresses in advanced occlusive lesions that takes the role of collateral circulatory pathways into account. For this purpose, a simplified methodology for evaluating MWSS in stenoses ranging from mild ones to occlusions is needed. Indeed, even if Navier–Stokes solvers are now very efficient to compute wall shear stress in moderate stenoses [11,13,14], some difficulties still remain for stenoses whose degree, expressed as percent narrowing in the luminal diameter, is higher than 70 percent. Moreover, achieving a new computation for every particular geometry and flow rate is still time consuming. Hence, Siegel et al. [13] have performed a regression analysis in order to interpolate their numerical results for all Reynolds numbers. However, the scaling law they have proposed is limited to three moderate constrictions (29, 50, and 69 percent radius reduction) and cannot be extrapolated to severe stenoses. There has been very little work toward a simplified method valid for severe stenoses, mainly done by Back et al. [15,16]. They used a local similarity method derived from the boundary-layer theory for steady flow through a conical axisymmetric constriction. However, they found that the wall shear stress monotonically increases from the inlet to the throat, whereas all other studies find a peak wall shear stress slightly upstream of the throat. Consequently, this model is only accurate for evaluating MWSS in approximately conical stenoses.

In the present study, the interactive boundary-layer (IBL) theory is applied. A scaling analysis based on geometric parameters (radius reduction at the throat and stenosis length) is achieved, assuming that the blood is Newtonian (viscosity of 0.03 Poise), the stenosis is axisymmetric with a small rate of change of taper and a smooth, rigid wall, and the flow is steady. Under these assumptions, widely used by others [11,13,14,16] and further discussed below, such an asymptotic method allows the extraction of the fundamental mechanisms and the determination of the relevant nondimensional parameters. In this way, a simple relationship is obtained between the MWSS in the convergence, the flow rate (or Reynolds number) and the geometric parameters. We thus compute the magnitude of MWSS in a carotid artery stenosis, as a function of the morphology of the circle of Willis and the stenotic pattern of both carotid arteries.

Methods

Stenosis Geometry. The stenosis geometry is approximated by an axisymmetric fourth-order polynomial (Fig. 1), defined by:

$$R(x) = -D\left(\frac{x}{L}\right)^4 + 2D\left(\frac{x}{L}\right)^2 + 1 - D, \quad x \in [-L, L], \qquad (1)$$

where x, R, and L are, respectively, the axial coordinate, the radial position of the wall, and the convergence length nondimensionalized by the upstream radius R_0^*, and D is the stenosis degree, i.e., radius reduction at stenosis throat.

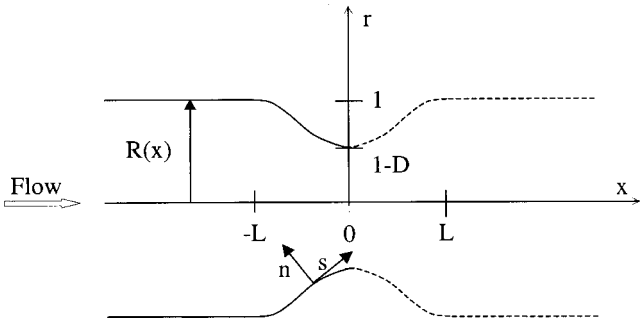

Fig. 1 Geometry and nondimensional parameters of stenosis

Wall Shear Stress in the Stenosis Convergent Part: IBL Integral Method. The IBL theory is based on two hypotheses. First, the Reynolds number based upon upstream diameter and mean upstream velocity (Re_0) is large enough (typically between 200 and 800) for the boundary-layer theory to hold. Second, as Re_0 is not strictly infinite, the boundary-layer at the vessel wall interacts with the potential (thus irrotational) core of inviscid fluid through the global conservation of flow [17–19]: The core flow speed is increased to take account of the boundary-layer displacement (at order $\mathrm{Re}_0^{-1/2}$), which is itself dependent on the pressure gradient in the core. This modification is a significant improvement on the classical boundary-layer approach, but even the IBL theory is only valid for attached flows.

Assuming a curvilinear system of coordinates (Fig. 1), we denote by s^* the current length measured along the stenosis wall from the beginning of the convergence ($x=-L$), n^* denoting the coordinate normal to the wall. The asymptotic dimensionless variables s, n, u, v, and u_e, are chosen to be of the same scale in the boundary-layer as Re_0 tends to infinity. They are determined by:

$$s=\frac{s^*}{R_0{}^*},\quad n=\frac{\sqrt{\mathrm{Re}_0}n^*}{\sqrt{2}R_0{}^*},\quad u=\frac{u^*}{\overline{u_0}{}^*},\quad v=\frac{\sqrt{\mathrm{Re}_0}v^*}{\sqrt{2}\overline{u_0}{}^*},\quad u_e=\frac{u_e{}^*}{\overline{u_0}{}^*}, \tag{2}$$

where u^*, v^*, and $u_e{}^*$ are, respectively, the velocity components parallel and normal to the wall, and the velocity at the edge of the boundary-layer. The displacement thicknesses of the boundary-layer are defined by:

$$\delta_1{}^*=\frac{\sqrt{2}R_0{}^*}{\sqrt{\mathrm{Re}_0}}\delta_1,\quad \delta_1=\int_0^\infty\left(1-\frac{u}{u_e}\right)dn. \tag{3}$$

Let us introduce new variables X, Y, Δ_1, U, V, and U_e defined by the Mangler transformation that reduces the problem to a plane bidimensional formulation [20]:

$$X=\int_0^s R(s')^2ds',\quad Y=R(s)n,\quad \Delta_1=R(s)\delta_1,\quad U=u,$$
$$V=\frac{1}{R(s)}\left(v+\frac{1}{R(s)}\frac{dR(s)}{ds}un\right),\quad U_e=u_e. \tag{4}$$

If the rate of change of taper of the convergence d^2R/dx^2 is everywhere small, the dimensionless versions of the boundary-layer equations [20] and of global conservation of flow, written in Mangler coordinates, are, respectively:

$$\left.\begin{aligned}&\frac{\partial U}{\partial X}+\frac{\partial V}{\partial Y}=0\\&U\frac{\partial U}{\partial X}+V\frac{\partial U}{\partial Y}=U_e\frac{dU_e}{dX}+\frac{\partial^2U}{\partial Y^2}\end{aligned}\right\} \tag{5}$$

and

$$U_e\left(R-\frac{\sqrt{2}\Delta_1}{R\sqrt{\mathrm{Re}_0}}\right)^2=1. \tag{6}$$

This system may be simplified by taking the integral form of the momentum equation, obtained by integrating it with respect to Y between 0 and infinity. Because d^2R/dx^2 is everywhere small, U is constant and equals U_e in the whole potential core. Thus, when Y tends to infinity, the velocity matches the velocity of the core. If Y is sufficiently high, the result of the integration is independent of the upper limit:

$$\frac{d}{dX}\left(\frac{\Delta_1}{H}\right)+\left(1+\frac{2}{H}\right)\Delta_1\frac{1}{U_e}\frac{dU_e}{dX}=\frac{f_2H}{\Delta_1U_e}, \tag{7}$$

where the shape factor H and the coefficient f_2 are defined by:

$$H=\Delta_1\left[\int_0^\infty\frac{U}{U_e}\left(1-\frac{U}{U_e}\right)dY\right]^{-1},\quad f_2=\frac{\Delta_1}{HU_e}\left.\frac{dU}{dY}\right|_{Y=0}. \tag{8}$$

To solve the set of ordinary differential equations (6) and (7) for Δ_1 and U_e, we need to calculate f_2 and H, and hence to hypothesize a suitable form for the velocity profile U. We suppose that the velocity profile may be locally approximated by one of the Falkner–Skan family (exact profiles for flow past wedges [21]). Thus, the role of the pressure gradient in the potential core (represented by Λ_1, see Eq. (9)) and the role of the no-slip condition at the wall are taken into account. The approximate closing laws, deduced from a Runge–Kutta 4 numerical integration of the self-similar equation, take the following form:

$$\Lambda_1=\Delta_1{}^2\frac{dU_e}{dX},$$

$$H=\begin{cases}2.59e^{-0.37\Lambda_1} & \Lambda_1<0.6\\ 2.07 & \Lambda_1\geqslant 0.6\end{cases},\quad f_2=0.94\left(\frac{4}{H^2}-\frac{1}{H}\right). \tag{9}$$

Given the stenosis geometry (i.e., L and D), the upstream displacement thickness δ_{1_0} and Reynolds number Re_0, the set of Eqs. (6) and (7) closed by Eq. (9) is numerically solved by a marching predictor/corrector method. The wall shear stress, τ_w (nondimensionalized by the upstream Poiseuille value $4\mu\overline{U_0}{}^*/R_0{}^*$, where μ is the viscosity), is obtained by:

$$\tau_w=\frac{1}{4\sqrt{2}}f_2H\frac{U_eR}{\Delta_1}\sqrt{\mathrm{Re}_0} \tag{10}$$

The value of MWSS is then computed. The relationship between MWSS and L, D, δ_{1_0} and Re_0 is investigated by regression analysis based on the least-squares method.

Simulation of Blood Flow Through the Circle of Willis. Once the relationship between MWSS and L, D, δ_{1_0} and Re_0 is known (see results), the calculation of MWSS in carotid stenoses requires knowledge of the trans-stenotic blood flow. As demonstrated by Cassot et al. [9], this flow rate is highly dependent on the anatomy of the circle of Willis.

Therefore, the blood flow through the distensible network including the circle of Willis and its afferent and efferent arteries (Fig. 2) is simulated as described by Zagzoule and Marc-Vergnes [22] and Cassot et al. [9]. In each segment of the network, a set of three unsteady equations (conservation of mass and momentum and purely elastic tube law) relates the variable cross-sectional area of the vessel, the pressure, the flow rate, and the wall shear stress. A second-order asymptotic expression of the wall shear stress as a function of the flow rate is provided to close the system [23]. The compatibility conditions at the nodes of the network are the identity of the pressure signals and the conservation of flow. The effects of the carotid stenoses are put into the network model by means of the semi-empirical formulas of Young, Tsai, and Seeley [24,25] relating the trans-stenotic pressure drop to the flow

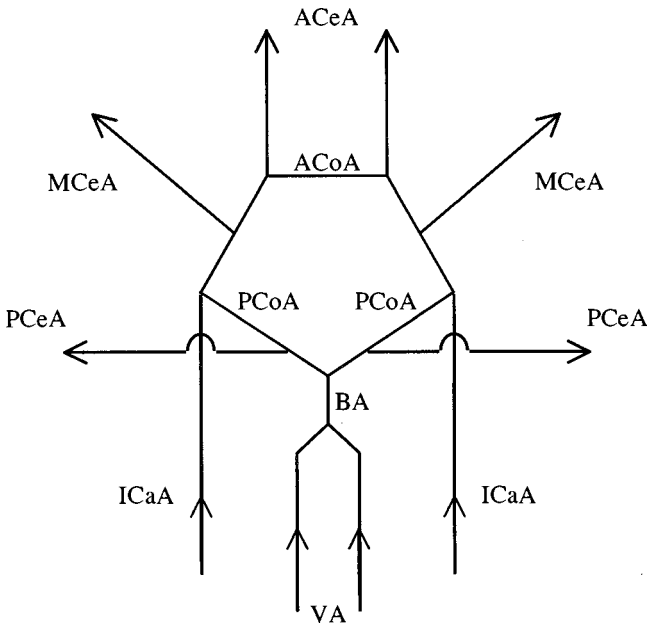

Fig. 2 Diagram of the circle of Willis and its afferent and efferent arteries. (VA: vertebral, BA: basilar, ICaA, internal carotid, ACeA: anterior cerebral, MCeA: middle cerebral, PCeA: posterior cerebral, ACoA: anterior communicating, PCoA: posterior communicating arteries.)

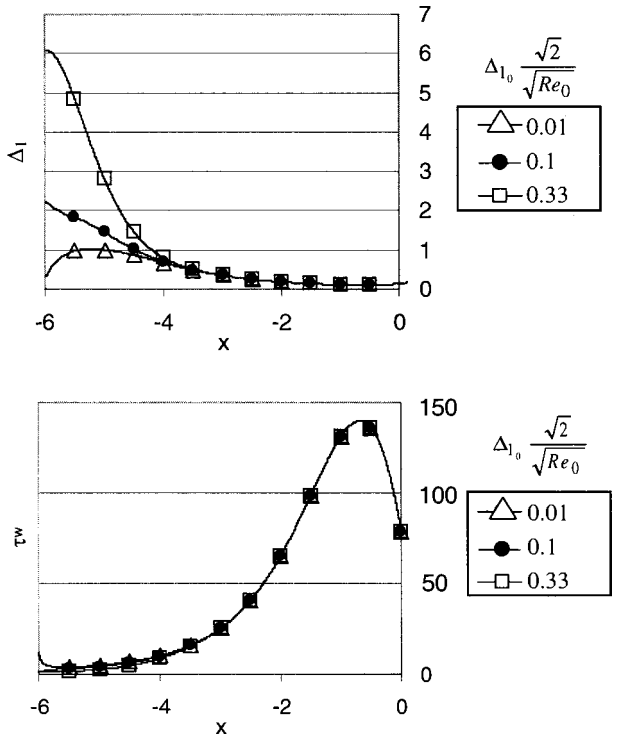

Fig. 3 Nondimensional displacement thickness in Mangler coordinates Δ_1 (upper) and wall shear stress (lower) versus axial position in the convergence characterized by $D=0.7$ and $L=6$, for $Re_0=1000$ and different values of $\Delta_{1_0}\sqrt{2}/\sqrt{Re_0}$ (corresponding to an initial displacement thickness $\delta_{1_0}^*$ between $0.01R_0^*$ and $0.33R_0^*$)

rate in streamlined constrictions. As the predicted pressure drop differs from the experimental measurements [26], the potential error associated with using these formulas is further discussed below.

By varying the diameters of anterior and posterior communicating arteries, within the range of anatomical data, we can simulate the hemodynamic influence of the circle of Willis. Stenoses of variable degrees can be added to one or to both internal carotid arteries ($R_0^*=2$ mm) over a 5 cm length (corresponding to $L=12.5$). Given the pressure signal at entries and outputs, the model computes instantaneous pressure and flow rate values at each point of the network. MWSS in the stenosed arteries is then derived from the average flow rate thus computed and the stenoses degrees.

Results

Validation of IBL Integral Method for Calculation of MWSS

1 Dependence on Upstream Displacement Thickness. Existence of a potential core implies that the displacement thickness δ_1^* is not thicker than $R_0^*R/3$ for a fully developed parabolic Poiseuille flow, i.e., from Eqs. (3) and (4):

$$\Delta_1 < \frac{R^2\sqrt{\mathrm{Re}_0}}{3\sqrt{2}}. \tag{11}$$

Therefore, the classical assumption of a fully developed parabolic flow at the inlet of the convergence [13,14] is not consistent with our methodology. Some authors [15,16] hypothesized a flat profile. Actually, the boundary-layer grows from the artery origin, and its thickness is unknown at the inlet of the constriction [27]. Therefore, the dependence of displacement thickness and wall shear stress distribution in the convergence on inlet displacement thickness was first investigated for nine values of Reynolds number (from 400 to 2000), thirteen values of D (from 0.3 to 0.9), and four values of L (from 3 to 12).

For example, Fig. 3 displays the results obtained in a 70 percent stenosis. Whatever the initial value of Δ_1, Eq. (11) holds and the curves of wall shear stress become superposed in the downstream part of the convergence, where the gradient parameter Λ_1 is greater than 0.6. Maximal difference from the mean for MWSS in all the cases studied is less than 0.25 percent. MWSS is therefore independent of inlet displacement thickness and thus, of the assumed entry velocity profile. This validates the use of the IBL theory.

2 Comparison With Solutions of Complete Navier–Stokes Equations. Siegel et al. [13] and Huang et al. [14] have numerically solved Navier–Stokes equations for axisymmetric Newtonian flow in moderate stenoses. In the first work, a spectral element method was applied to cosine-shaped constrictions ($L\in[3;6]$ and $D\in[0.29;0.5;0.69]$) for diverse Reynolds number values. Huang et al. [14] used a finite difference scheme with an unspecified constriction shape, for five values of pair (L, D) ((2, 0.25), (2, 0.33), (2, 0.5), (4, 0.5), (1, 0.5)), and three values of Re_0 (100, 500, 1000). The results obtained with both methods are consistent with our IBL method: the discrepancy between the various MWSS obtained for the same stenotic configuration (e.g., same values of pairs (L, D)) is smaller than 8.5 percent in spite of different shapes of the stenosis model.

Scaling Law for Maximal Wall Shear Stress. Siegel et al. [13] performed a scaling analysis of the numerical results obtained in three moderate constrictions (29, 50, and 69 percent radius reduction), leading to the following relationship:

$$\mathrm{MWSS}=a(\mathrm{Re}_0)^{0.5}+b, \tag{12}$$

where the numerical values of coefficients a and b depend on stenosis degree and length in an unknown fashion. Our aim was to complete these results for stenoses ranging from moderate to severe ones, focusing on dependence of MWSS on the upstream

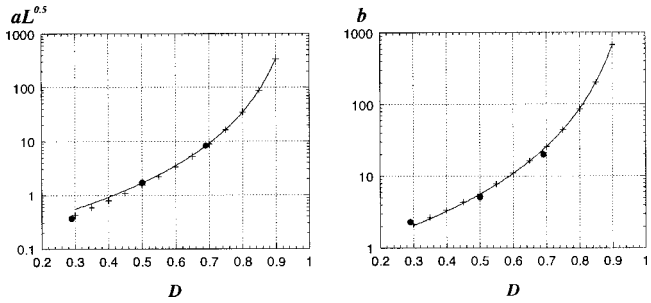

Fig. 4 Parameters $a(L)^{0.5}$ and b as a function of radius reduction. Full circles: results derived from Siegel et al. [13]; cross: mean of the results of regression analysis obtained for L between 3 and 12 at fixed D; line: interpolation of results averaged upon L.

Reynolds number and the geometric parameters. In other words, we investigated the dependence of parameters a and b (Eq. (12)) on stenosis length and radius reduction. The first step was to analyze the dependence of MWSS on Re_0 for D between 0.3 and 0.9 and L between 3 and 12. Regression analysis of the results showed that this dependence is correctly described by Eq. (12). The correlation coefficient in all cases was 0.999 or greater. Finally, we looked for a relationship between the thus identified a and b coefficients and the corresponding values of L and D. As indicated by the dimensional analysis of Eq. (10) (see Appendix A), $a\sqrt{L}$ and b should be independent of L. This was verified, as the maximal deviation from the mean values of $a\sqrt{L}$ and b obtained for a range of L (3 to 12) at fixed D was 1.1 percent and 2.9 percent, respectively. Hence, a relationship between these averaged $a\sqrt{L}$ and b parameters and D alone (see Fig. 4) was sought. The chosen fitting function, derived from the dimensional analysis of Eq. (10) (see Appendix A), was:

$$\frac{K}{(1-D)^{\xi}}, \tag{13}$$

where K and ξ are positive real numbers. Results obtained by the least squares method are given in Table 1, and displayed in Fig. 4. They show very good agreement with numerical values derived from Siegel et al. [13].

Finally, the generalized law for MWSS is:

$$\mathrm{MWSS}=\frac{0.170}{(1-D)^{3.298}}\frac{{\mathrm{Re}_0}^{0.5}}{L^{0.5}}+\frac{0.705}{(1-D)^{2.984}}. \tag{14}$$

Table 1 Estimated parameters K and ξ (see Eq. (13)) and regression coefficients

	K	ξ	χ square	Correlation coefficient
$a(L)^{0.5}$	0.170	3.298	0.291	1.000
b	0.705	2.984	0.146	1.000

Hence, dimensional expression as a function of parameters measurable in clinical practice is the following:

$$\mathrm{MWSS}^*=\frac{4\mu Q^*}{\pi({R_0}^*)^3}\left(\frac{0.240}{(1-D)^{3.298}}\frac{1}{L^{0.5}}\left(\frac{Q^*}{\pi {R_0}^*\nu}\right)^{0.5}+\frac{0.705}{(1-D)^{2.984}}\right), \tag{15}$$

where Q^* is the flow rate through the stenosis.

MWSS in a Carotid Stenosis: Role of the Patency of the Circle of Willis and of Stenotic Pattern. Cassot et al. [9] have shown that the flow rate in a carotid stenosis is highly dependent on its radius reduction and, provided collateral circulatory pathways of the circle of Willis are efficient, on stenosis degree at the contralateral side. Hence, dependence of MWSS* on these parameters was investigated.

1 MWSS Dependence on Carotid Stenosis Degree. Figure 5, left, displays the variations of MWSS* in a unilateral stenosis versus stenosis degree for five configurations of the circle of Willis, i.e., for five arrangements of anterior communicating arteries (ACoA) and posterior communicating arteries (PCoA) diameters. Whatever the configuration, MWSS* exhibits a maximal value for a stenosis degree between 60 and 80 percent. The maximal value of MWSS* depends on the configuration of the circle of Willis: It is multiplied by approximately four when both communicating arteries are narrow (ACoA and PCoA diameter equal to 0.4 mm) compared to the cases when one of the communicating arteries at least is broad (diameter equals to 1.6 mm), which allows collateral supply from anterior and/or posterior territories.

In the case of a stenosis associated with a contralateral occlusion (Fig. 5, right), the higher MWSS* is obtained when the ACoA is broad and the PCoA is narrow, because the nonoccluded carotid irrigates ipsi- and contralateral anterior cerebral territories, without collateral supply from the posterior side. The greater the caliber of the PCoA, the smaller the maximal value of the MWSS*.

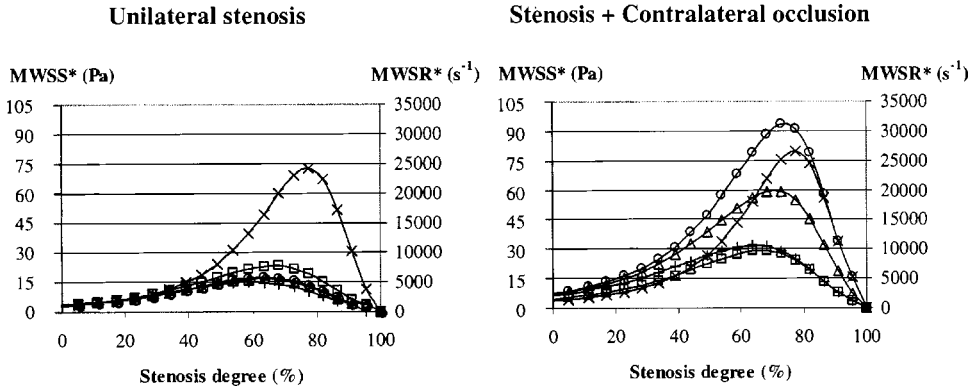

Fig. 5 Dimensional maximal wall shear stress (MWSS*) and rate (MWSR*) as a function of stenosis degree, for five arrangements of anterior and posterior communicating arteries diameters; ×: AcoA=0.4 mm/PCoA=0.4 mm; □: ACoA=0.4 mm/PCoA=1.6 mm; ○: ACoA=1.6 mm/PCoA=0.4 mm; △: ACoA=1.6 mm/PCoA=1 mm; +: ACoA=1.6 mm/PCoA=1.6 mm.

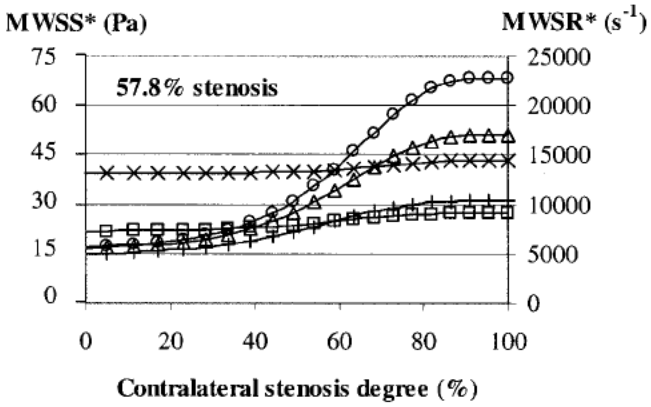

Fig. 6 Dimensional maximal wall shear stress (MWSS*) and rate (MWSR*) in a 57.8 percent stenosis as a function of contralateral stenosis degree, for five arrangements of anterior and posterior communicating arteries diameters; same symbols as Fig. 5

2 MWSS Dependence on Contralateral Stenosis Degree. As an example, Fig. 6 displays the variations of MWSS* in a 57.8 percent radius reduction stenosis versus contralateral stenosis degree for five configurations of the circle of Willis. In all cases, an S-shaped curve is obtained. As long as the degree of the contralateral stenosis remains less than 30 percent, the MWSS* value does not change significantly from the value for a unilateral stenosis, while contralateral stenoses greater than 80 percent have practically no further effects on the MWSS*, and behave like occlusions. As the degree of the contralateral stenosis increases from 30 percent to 80 percent, the MWSS* increases, but the slope of the curve is strongly affected by the communicating arteries' diameters: It increases when ACoA diameter increases, because the interaction between ipsilateral and contralateral sides increases, and decreases when PCoA diameter increases, because collateral supply from the posterior territories minimizes flow rate augmentation. Consequently, when the ACoA is thin, the amplitude of the S-shaped curve is almost zero. Maximal amplitude is obtained for broad anterior and thin posterior arteries, leading to very high MWSS* in moderate stenoses (up to 70 Pa for a 60 percent stenosis). When the degree of contralateral stenosis equals the degree of the ipsilateral one, the cerebral network presented in Fig. 2 becomes symmetric, and ACoA diameter has no influence. Curves obtained for the same PCoA intersect in that case, whatever ACoA patency.

Discussion

Our scaling law for MWSS in a stenosis is based on several simplifications when compared to the pathophysiological complexity. The principal assumptions are to consider the blood as a Newtonian fluid, the flow as steady, and the stenosis as axisymmetric with a small rate of change of taper and a smooth, rigid wall. Nevertheless, even if blood is non-Newtonian, its non-Newtonian components do not affect the magnitude of wall shear stresses in arterial conditions [28]. The relative error made when calculating the MWSS assuming quasi-steadiness of the flow instead of taking its unsteadiness into account can be evaluated by a dimensional analysis from Pedley [29] taking numerical data found in carotid arteries [9,22]. This error is about 15, 10, 7, and 5 percent for respectively a 30, 50, 70, and 85 percent stenosis. As intimal thickening in stenosed arteries decreases the flexibility of the wall, the variations of stenosis radius caused by pressure fluctuations encountered in carotids [22], are less than 1.5 percent. The hypothesis of a little rate of change of taper is not limiting, since it is verified even for total occlusions if $L \geqslant 3$, i.e., if the convergence length is greater than 6 mm. The two last assumptions are the axisymmetric and smooth geometry. However, they made possible the dimensional analysis (Appendix A), which explained the simple dependence of MWSS on geometrical parameters and Reynolds number. The results of Siegel et al. [13] were explained and extended to a larger range of stenosis degrees (in particular for severe ones), with a simpler methodology and a great reduction in computing time. The main interest of the so-obtained scaling law (Eq. (14) or (15)) is that all the parameters needed are measurable either in *in vitro* experiments, or in clinical practice, allowing a simple and much more accurate evaluation of MWSS than the classical Poiseuille law. This could be of greatest concern for studying the role of elevated shear stresses in advanced occlusive lesions, particularly on plaque ulceration, rupture, and thromboembolism.

Using our scaling law, we calculated MWSS values in carotid stenoses, according to the patency of collateral pathways. The main assumption in the simulation of blood flow through the circle of Willis was to use semi-empirical formulas of Young, Tsai, and Seeley relating the trans-stenotic pressure drop to the flow rate in streamlined constrictions. As the predicted pressure drop differs from the experimental measurements [26], the potential error associated with using these formulas was estimated in the particular case where both anterior and posterior communicating arteries are so narrow that they functionally behave as closed. This analysis demonstrated that using more accurate formulas would change the absolute numbers, but not the general trends of the results depicted in Figs. 5 and 6. As an example, the maximal MWSS* calculated when both communicating arteries are narrow (ACoA and PCoA diameter equal to 0.4 mm) is underestimated by around 35 percent.

An interesting result is that wall shear stress doesn't increase monotonically with the stenosis degree: The stenosis degree leading to maximal MWSS results from a balance between the increase of wall shear stress due to increasing velocity, in order to satisfy mass conservation, and its decrease due to reduction of flow rate through the vessel induced by its increased resistance. This suggests that risk of embolus release could be greater for some moderate stenoses than for more severe ones. Even for a given stenosis degree, the results show huge variations of the MWSS. For instance, very high MWSS* values (>70 Pa) can be found in moderate stenoses (60 percent), if they are associated with a contralateral occlusion, large ACoA, and narrow PCoA diameters. This last result was obtained because we have not only considered an isolated stenosed vessel, but also included it in the whole network. It could explain the uncertainty about the percentage of stenosis above which carotid obstructive lesions must be considered severe for the risk of stroke. In fact, peril of embolic stroke is likely to be elevated for stenosis degree where MWSS is maximal (i.e., between 60 and 80 percent), when risk of hemodynamic stroke increases with stenosis degree. Further investigations on the mechanical properties of thrombi and plaques are therefore needed for a better understanding of the role of MWSS in the embolic mechanisms.

Acknowledgments

The authors gratefully acknowledge Mokhtar Zagzoule, Eduardo Anglés-Cano, and Stanley Berger for enlightening discussions. This work was supported by a research grant (4M101C) from INSERM (French National Institute for Health and Medical Research) Intercommission No. 1 and by the CNRS (French National Center for Scientific Research).

Nomenclature

a, b = coefficients for maximal wall shear stress relationship (Eq. (12))
D = degree of stenosis (radius reduction at stenosis throat)
L = length of convergent part of stenosis
n = coordinate at right angle to the stenosis wall

Q = flow rate
R = radial position of the wall
Re_0 = Reynolds number based upon upstream diameter and mean upstream velocity $= 2R_0^* \cdot \overline{U_0^*}/v = 2Q^*/\pi R_0^* v$
s = current length measured along the stenosis wall from the beginning of the convergence ($x = -L$)
u = velocity component parallel to the stenosis wall
U = velocity component in the Mangler X direction
v = velocity component normal to the stenosis wall
V = velocity component in the Mangler Y direction
x = axial coordinate
X, Y = Mangler coordinates (see Eq. (4))
δ_1 = displacement thickness of the boundary-layer
Δ_1 = displacement thickness of the boundary-layer in Mangler coordinates
Λ_1 = pressure gradient parameter of the boundary-layer
μ = viscosity
v = kinematic viscosity
τ_w = wall shear stress

Subscripts

0 = upstream condition ($x = -L$)
e = condition at the edge of the boundary-layer

Superscripts

— = mean over a cross section
* = dimensional quantities
none = nondimensional quantities

Appendix A: Dependence of MWSS on Parameters

In order to analyze the dependence of MWSS on geometrical parameters and Reynolds number, a dimensional analysis was performed. Wall shear stress as a function of these parameters is given by Eq. (10). Since MWSS is obtained in the part where the gradient parameter Λ_1 is greater than 0.6 (see Results), implied in Eq. (9) is that f_2 and H are constants. As:

$$\frac{\Delta_1}{R\sqrt{\mathrm{Re}_0}} \ll R, \tag{A.1}$$

simplification of Eq. (6) gives at first order:

$$U_e \approx \frac{1}{R^2}\left(1 + 2\sqrt{2}\,\frac{\Delta_1}{R^2\sqrt{\mathrm{Re}_0}}\right). \tag{A.2}$$

The basic assumption of boundary-layer theory [20] gives, for the displacement thickness:

$$\delta_1^*(x^*) \approx \frac{s^*}{\sqrt{\mathrm{Re}(s^*)}}, \tag{A.3}$$

where $\mathrm{Re}(s^*)$ is the *local* Reynolds number in the potential core, based on $s^*(x^*)$ and $u_e^*(x^*)$. Assuming that the axial location of the MWSS is near the throat, combination of Eqs. (3), (4), and (A.3) leads to:

$$\Delta_1 \approx \frac{R\sqrt{L}}{\sqrt{U_e}}. \tag{A.4}$$

Thus, by use of Eqs. (A.2) and (A.4), Eq. (10) at first order reduces to:

$$\mathrm{MWSS} \approx k\left(\frac{1}{R_{\mathrm{throat}}{}^3}\,\frac{\sqrt{\mathrm{Re}_0}}{\sqrt{L}} + \frac{3\sqrt{2}}{R_{\mathrm{throat}}{}^3}\right), \tag{A.5}$$

where k is a real constant and $R_{\mathrm{throat}} = (1 - D)$.

References

[1] Mohr, J P , Caplan, L R , Melski, J W , Goldstein, R J , Duncan, G W , Kistler, J P , Pessin, M S , and Bleich, H L , 1978, ''The Harvard Cooperative Stroke Registry: A Prospective Registry,'' Neurology, **28**, pp 754–762
[2] Bogousslavski, J , Van Melle, G , and Regli, F , 1988, ''The Lausanne Stroke Registry: Analysis of 1000 Consecutive Patients With First Stroke,'' Stroke, **19**, pp 1083–1092
[3] NASCET, 1991, ''North American Symptomatic Carotid Endarterectomy Trial Collaborators Beneficial Effect of Carotid Endarterectomy in Symptomatic Patients With High Grade Stenosis,'' N Engl J Med , **325**, pp 445–453
[4] ECST, 1991, ''European Carotid Surgery Trialists' Collaborative Group: MRC European Surgery Trial: Interim Results for Symptomatic Patients With Severe (70–99 Percent) or With Mild (0–29 Percent) Carotid Stenoses,'' Lancet, **337**, pp 1235–1243
[5] Schomer, D F , Marks, M P , Steinberg, G K , Johnstone, I M , Boothroyd, D B , Ross, M R , Pelc, N J , and Enzmann, D R , 1994, ''The Anatomy of the Posterior Communicating Artery as a Risk Factor for Ischemic Cerebral Infarction,'' N Engl J Med , **330**, pp 1565–1570
[6] Ringelstein, E B , Weiller, C , Weckesser, M , and Weckesser, S , 1994, ''Cerebral Vasomotor Reactivity Is Significantly Reduced in Low-Flow as Compared to Thromboembolic Infarctions: The Role of the Circle of Willis,'' J Neurol Sci , **121**, pp 103–109
[7] Sitzer, M , Müller, W , Siebler, M , Hort, W , Kniemeyer, H W , Jäncke, L , and Steinmetz, H , 1995, ''Plaque Ulceration and Lumen Thrombus Are the Main Sources of Cerebral Microemboli in High-Grade Internal Carotid Artery Stenosis,'' Stroke, **26**, pp 1231–1233
[8] Sakariassen, K S , and Barstad, R M , 1993, ''Mechanisms of Thromboembolism at Arterial Plaques,'' Blood Coagul Fibrinolysis, **4**, pp 615–625
[9] Cassot, F , Vergeur, V , Bossuet, P , Hillen, B , Zagzoule, M , and Marc-Vergnes, J P , 1995, ''Effects of Anterior Communicating Artery Diameter on Cerebral Hemodynamics in Internal Carotid Artery Disease: A Model Study,'' Circulation, **92**, pp 3122–3131
[10] Ku, D , Giddens, P , Zarins, C , and Glagov, S , 1985, ''Pulsatile Flow and Atherosclerosis in the Human Carotid Bifurcation: Positive Correlation Between Plaque Location and Low and Oscillating Shear Stress,'' Arteriosclerosis Dallas, **5**, pp 293–302
[11] Bluestein, D , Niu, L , Schoephoerster, R T , and Dewanjee, M K , 1997, ''Fluid Mechanics of Arterial Stenoses: Relationship to the Development of Mural Thrombus,'' Ann Biomed Eng , **25**, pp 344–356
[12] Nerem, R M , 1992, ''Vascular Fluid Mechanics, the Arterial Wall and Atherosclerosis,'' ASME J Biomech Eng , **114**, pp 274–282
[13] Siegel, J M , Markou, C P , Ku, D N , and Hanson, S R , 1994, ''A Scaling Law for Wall Shear Stress Through an Arterial Stenosis,'' ASME J Biomech Eng , **116**, pp 446–451
[14] Huang, H , Modi, V J , and Seymour, B R , 1995, ''Fluid Mechanics of Stenosed Arteries,'' Int J Eng Sci , **33**, pp 815–828
[15] Back, L H , 1975, ''Theoretical Investigation of Platelet Embolus Production in Atherosclerotic Coronary Arteries,'' Math Biosci , **25**, pp 273–307
[16] Back, L H , and Crawford, D W , 1992, ''Wall Shear Stress Estimates in Coronary Artery Constrictions,'' ASME J Biomech Eng , **114**, pp 515–520
[17] Le Balleur, J C , 1978, ''Couplage Visqueux Non-Visqueux: Méthode Numérique et Applications aux Écoulements Bidimensionnels Transsoniques et Supersoniques,'' La Recherche Aérospatiale 1978-2, pp 67–76, Eng Trans ESA TT-496
[18] Cousteix, J , 1988, *Couche Limite Laminaire*, Editions Cepadues, Toulouse
[19] Cebeci, T , and Cousteix, J , 1999, *Modeling and Computation of Boundary-Layer Flows*, Springer, Berlin
[20] Schlichting, H , 1979, *Boundary-Layer Theory*, 7th ed , McGraw-Hill, New York
[21] Gersten, K , and Hervig, H , 1992, *Strömungsmechanik: Grundlagen der Impuls-, Wärme und Stoffübertragung aus Asymptotischer Sicht*, Vieweg, Wiesbaden
[22] Zagzoule, M , and Marc-Vergnes, J P , 1986, ''A Global Mathematical Model of the Cerebral Circulation in Man,'' J Biomech , **19**, pp 1015–1021
[23] Zagzoule, M , Khalid-Naciri, J , and Mauss, J , 1991, ''Unsteady Wall Shear Stress in a Distensible Tube,'' J Biomech , **24**, pp 435–439
[24] Seeley, B D , and Young, D F , 1976, ''Effect of Geometry on Pressure Losses Across Models of Arterial Stenoses,'' J Biomech , **9**, pp 439–448
[25] Young, D F , 1979, ''Fluid Mechanics of Arterial Stenoses,'' ASME J Biomech Eng , **101**, pp 157–179
[26] Young, D F , and Tsai, F Y , 1973, ''Flow Characteristics in Models of Arterial Stenoses I Steady Flow,'' J Biomech , **6**, pp 395–410
[27] Kerber, C , and Liepsch, D , 1994, ''Flow Dynamics for Radiologists Basic Principles of Fluid Flow,'' AJNR Am J Neuroradiol , **15**, pp 1065–1075
[28] Brookshier, K , and Tarbell, J , 1991, ''Effect of Hematocrit on Wall Shear Rate in Oscillatory Flow: Do the Elastic Properties of Blood Play a Role?'' Biorheology, **28**, pp 569–587
[29] Pedley, T J , 1972, ''Two-Dimensional Boundary Layer in a Free Stream Which Oscillates Without Reversing,'' J Fluid Mech , **55**, pp 359–383